Theoretical insights on the electroluminescent mechanism of thermally activated delayed fluorescence emitters

CrossMark

Lili Lin, Zhongjie Wang[*], Jianzhong Fan, Chuankui Wang[**]

Shandong Province Key Laboratory of Medical Physics and Image Processing Technology, Institute of Materials and Clean Energy, School of Physics and Electronics, Shandong Normal University, 250014 Jinan, China

ABSTRACT

Thermally activated delayed fluorescence (TADF) emitters, with internal quantum efficiency (IQE) in organic light-emitting diodes (OLED) approaching 100%, have attracted great attention recently. However, theoretical investigation on the electroluminescent mechanism of TADF emitters is quite rare. In this paper, the time-dependent density functional theory is used to study the property of excited states of the TADF emitters, and it is found that both the geometry and the electronic structure are quite dependent on the functionals. By comparing with the experimental results, a 'hybrid' method is adopted to study the photophysical properties of the TADF emitters. Based on the energy structure of the states, the lowest three states are found to have close relation to the electroluminescent process. The dynamics of two lowest excited states are investigated and the rate equation is used to analyze the evolution of the three states involved. A visual picture of the exciton evolution process is obtained, and one can get a better understanding of the up-conversion mechanism of TADF emitters. The analysis of the electron distribution of the transition orbitals indicates that the first singlet excited state of the molecule possesses both the charge transfer and local excitation components, which is a necessary character for a TADF emitter. The comparison of the property of two isomers indicates that the appropriate arrangement of donor groups and acceptor groups is important for a high-efficient TADF emitter.

© 2016 Elsevier B.V. All rights reserved.

1. Introduction

Organic light-emitting diodes (OLED), due to their lightness, flexibility, low-cost, self-lighting et al., have attracted much attention recently. However, the low-efficiency has long been one of the reasons that hindered the development and application of the OLED. The efficiency of the OLED is closely determined by the internal quantum efficiency (IQE) of organic light-emitting molecular materials which are the main components of the OLED. Therefore, it is desirable to design and apply the organic light-emitting molecules with high IQE. The IQE of the organic electroluminescent molecules is determined by three factors. One is the efficiency to form excitons from recombination of the injecting electrons and holes. The other is the utilizing efficiency of the singlet excitons, and the last one is the fluorescence efficiency of the singlet

excitons. According to spin statistics, the ratio of singlet and triplet excitons generated is 1:3 [1]. It is generally believed that the internal quantum efficiency of organic light-emitting molecules can not exceed 25%. Recently, nearly 100% IQE of OLED is realized by enhancing the reverse intersystem crossing (RISC) of the triplet state excitons→singlet state excitons (T1→S1) [2]. This novel pathway has attracted wide attention, and some groups have successfully enhanced the electroluminescence efficiency by this way [3]. Professor Ma's group provided an evidence of the RISC in the organic light-emitting molecules by using the magneto-electroluminescence measurement [4]. However, theoretical study on the RISC mechanism is quite rare and it is still not clear how the RISC is realized for specific emitters [5].

Generally speaking, the RISC process is determined by the spin-orbit coupling (SOC) and the energy gap between the S1 state and the T1 state ($k \propto \frac{V_{ij}}{\Delta E_{ST}}$, V_{ij} is the SOC). It is known that SOC for the organic molecules is quite weak. If SOC is zero, it is impossible to realize the RISC process, even though the S-T energy gap is quite small. Consequently, it is necessary to obtain the SOC value theoretically. In addition, to enhance the RISC, it is necessary to reduce

the energy gap between S1 and T1. One useful way is to separate the electron distribution of transition orbitals involved in S1 by designing molecules composed of donor (D) groups and acceptor (A) groups. However, this will directly weaken radiation decay rate. Thus, to decrease the S-T energy gap and to enhance the radiation rate conflict with each other, and it is delicate work to design one molecule satisfying both two conditions. A series of molecules based on carbazolyl dicyanobenzene (CDCB), with carbazole as a donor and dicyanobenzene as an electron acceptor are found to have nearly 100% internal quantum efficiency based on the RISC mechanism [2]. It is quite meaningful and necessary to investigate how these two conditions are satisfied and how the RISC process is realized.

In this study, the time-dependent density functional theory (TD-DFT) will be used to study the property of the excited states. As both the geometric structures and the electronic structures of molecules are tightly dependent on the functional used, various functionals are tested first based on the 2CzPN molecule (see Fig. 1(a), composed of two carbazolyl groups and one dicyanobenzene group). The functional, appropriate to describe this kind of system, will be determined. Following that, the systematic study on the geometric character and the property of excited states are performed for the 4CzIPN molecule (see Fig. 1(b), composed of four carbazolyl groups and one dicyanobenzene group. Further, the dynamics of excited states including the intersystem crossing,

internal conversion and non-radiation transition processes is also investigated. In addition, the rate equation is used to study the conversion process of the excited states, and a visual picture of the up-conversion process will be presented. At last, the 4CzPN molecule (see Fig. 1(c)), the isomer of the 4CzIPN molecule, is also studied, which will give some enlightenment on the design of TADF emitters.

2. Calculation methods

In this paper, the geometry optimization and the calculation of electronic structures for the ground state and the excited states of the molecules are performed with the density functional theory (DFT) and the TD-DFT method. The B3LYP, Cam-B3LYP, PBE0, M06-2X and WB97X-D functionals are used to optimize the geometry of the 2CzPN molecule. Both B3LYP and M06-2X are adopted in the study of the 4CzIPN and 4CzPN molecule (see Fig. 1(c)). In comparison with the experimental results, a 'hybrid' method which combines the M06-2X functional and the B3LYP functional is adopted. Specifically, the calculation of the energy is performed with B3LYP and the geometry structure adopts the results obtained with M06-2X. The basis set 6-31G* is used in all the first-principles calculations which are realized in Gausssian 09 program [6]. The electron and hole distribution of the S1 state is analyzed using the multifunctional wavefunction analyzer (Multiwfn) [7].
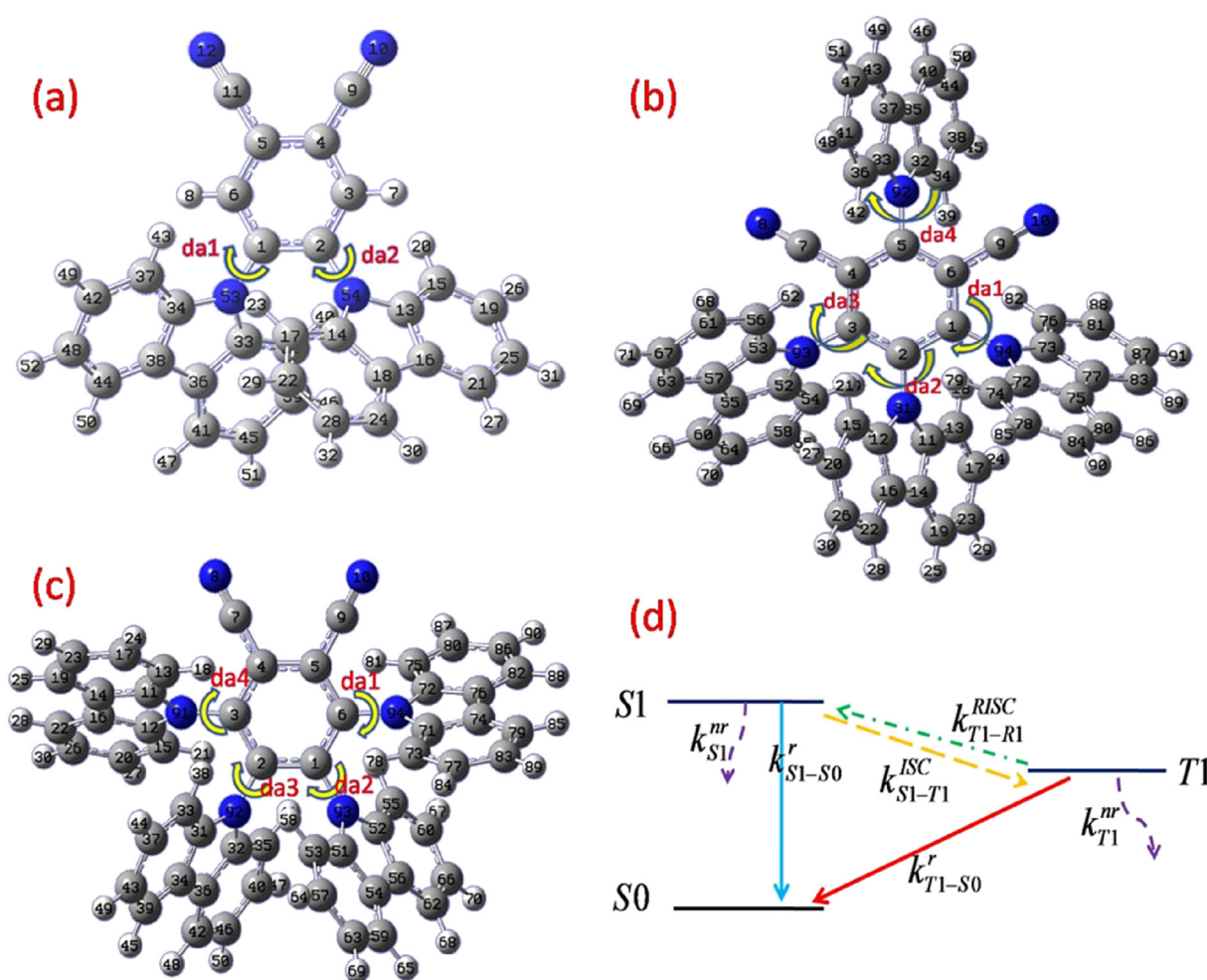

Fig. 1. Geometry structure of the 2CzPN molecule (a), the 4CzIPN molecule (b), and the 4CzPN molecule (c). (d) Diagram of three states studied in our study. The transition rates involved are also labeled.

For the 4CzIPN molecule, the dynamics of the excited states are also studied. According to the characteristic of the energy structure of the molecule (see Fig. S1), three states including the S0, S1 and T1 states are studied (see Fig. 1(d)). The dynamic processes involve the radiation decay of the S1 state (k_{S1-S0}^r), the non-radiation decay of the S1 and T1 states (k_{S1-S0}^{nr} and k_{T1-S0}^{nr}), the (Reverse) intersystem crossing (k_{S1-T1}^{ISC} (k_{T1-S1}^{RISC})) and the radiation of the T1 state (k_{T1-S1}^r). To analyze the evolution process, the rate equation is used.

$$\frac{d\rho_{S0}}{dt} = \rho_{S1}k_{S1-S0}^r + \rho_{S1}k_{S1}^{nr} + \rho_{T1}k_{T1-S0}^r + \rho_{T1}k_{T1}^{nr}$$

$$\frac{d\rho_{S1}}{dt} = -\rho_{S1}k_{S1-S0}^r - \rho_{S1}k_{S1}^{nr} - \rho_{S1}k_{S1-T1}^{ISC} + \rho_{T1}k_{T1-S1}^{RISC} \qquad (1)$$

$$\frac{d\rho_{T1}}{dt} = -\rho_{T1}k_{T1-S0}^r - \rho_{T1}k_{T1}^{nr} - \rho_{T1}k_{T1-S1}^{RISC} + \rho_{S1}k_{S1-T1}^{ISC}$$

In Equation (1) ρ_{S0}, ρ_{S1} and ρ_{T1} are population number of the S0, S1 and T1 states, and the initial value for them are assumed as 0.0, 0.25 and 0.75 respectively.

In this paper, the fluorescence rate (or the radiation decay rate of the S1 state) is calculated using the Einstein spontaneous emission rate formula [8].

$$k_{S1-S0}^r = \frac{f\Delta E^2}{1.499} \qquad (2)$$

where f is oscillator strength from S1 state to S0 state, ΔE is the energy difference between the S1 state and the S0 state, which is in the unit of cm^{-1}.

The non-radiation decay of the S1 state and T1 state to the ground state can be evaluated with MOMAP program [9], detail calculation formula can refer to Ref. [10]. The (R)ISC is also one kind of non-radiation decay. To simplicity, the (R)ISC decay rates are calculated with the classical Marcus rate equation.

$$k_{ji} = \frac{V_{ji}^2}{\hbar}\sqrt{\frac{\pi}{K_BT\lambda}}\cdot\exp\left[-\frac{(\Delta G_{ji}+\lambda)^2}{4\lambda K_BT}\right] = \frac{V_{ji}^2}{\hbar}\sqrt{\frac{\pi}{K_BT\lambda}}\cdot\exp\left[-\frac{\Delta G^\perp}{K_BT}\right] \qquad (3)$$

Here, K_B is Boltzmann constant and T is the temperature. V_{ij} is the spin-orbit coupling between the S1 state and the T1 state, and T is the temperature which is set as 300 K here. In the active energy ($\Delta G^\perp = \frac{(\Delta G_{ji}+\lambda)^2}{4\lambda}$), ΔG_{ij} the energy difference between the S1 state and the T1 state and λ is the reorganization involving both the S1 state and T1 state. In calculation of the ISC rate, $\Delta G_{ij} = E_{T1} - E_{S1}$. The parameters involved are all calculated based on the first-principles calculations. The spin-orbit coupling between S1 and T1 is calculated with quadratic response function methods [11], which can be realized with the Dalton program [12]. In addition, the radiation decay rate of T1 can also be realized in Dalton program, and one can refer to Ref.11 to see the details.

3. Results and discussions

3.1. Functional test

In this study, the DFT method is used to study the electronic property of the organic molecules and the property of the organic molecules is tightly associated with the functionals used. Thus, one important work is to determine the functional before calculations. To save the computational cost, the 2CzPN molecule is tested with different functionals. The geometries of the 2CzPN molecule optimized with five different functionals have significant differences in

the dihedral angles between the carbazolyl groups (D) and the dicyanobenzene group (A), especially for the S1 state and the T1 state (see Table S1). As we can see, the angles **da1** and **da2** have little differences for both the S0 state and the S1 state obtained with the B3LYP, Cam-B3LYP and PBE0 functionals. While the two kinds of angles obtained with M06-2X and WB97X-D are very different from them. The angles **da1** and **da2** for the S1 state obtained with B3LYP, Cam-B3LYP and PBE0 are almost 90°. However, they are 86.87 and 71.31° obtained with M06-2X. The geometry obtained with WB97X-D is quite similar to that obtained with M06-2X. For the T1 state, the **da1** and **da2** obtained with the B3LYP functional still tend to 90°, while they deviate from the vertical state when the molecules are optimized with other four kinds of functionals. For comparison, the geometric structures for S0, S1 and T1 states optimized with B3LYP and M06-2X are shown in Fig. S2 and Fig. S3 respectively. Both the front view and the side view are presented. As we can see that the geometry of the ground state optimized with B3LYP has a little difference with that obtained at M06-2X level. While the S1 and T1 states optimized at two levels are quite different with each other. From the side view and front view, we find that the geometry of the S1 state and the T1 state optimized with B3LYP adopt approximately symmetric structures. Nevertheless, they are not symmetric when they are optimized with M06-2X. Besides, there are significant differences between the S0 and S1 states at the B3LYP computational level, while the difference is smaller for them obtained with M06-2X and WB97X-D.

The excitation energy of the S1 state and the T1 state calculated with five kinds of functionals are shown in Table 1. It is indicated that the excitation energies for both S1 and T1 state calculated with B3LYP are relatively smaller than the values obtained with other functionals. The energy gap between the S1 and T1 states is also strongly dependent on the functionals. The energy gap calculated with B3LYP is 0.335 eV, while it is as large as 0.957 eV in the situation of Cam-B3LYP. The energy gap calculated with M06-2X is 0.501 eV, which is smaller than that calculated with WB97X-D. In addition, the emission wavelengths λ_{em} in gas phase calculated with various functionals are also shown in Table 1. The wavelength calculated with B3LYP is 672 nm, which is quite larger than the experimental value (473 nm) [2]. The value calculated with M06-2X is 446 nm, in much better agreement with the experimental result. Further, the oscillator strengths of the S1 state calculated with different functionals are also shown in Table 1. It indicates that the values of the oscillator strength calculated with the B3LYP, Cam-B3LYP and PBE0 functionals are 0.0001, which indicates that the S1 state almost can't emit light. The values calculated with the M06-2X and WB97X-D functionals are relatively large, although they are still smaller than the normal fluorescent emitters.

As the S-T energy gap for TADF emitters should be smaller than the 0.1eV, it is much larger than 0.1 eV for the 2CzPN molecule in our investigation. This deviation may be due to that the functionals are not suitable to describe the system. Based on our calculation results, we can see that the energy gap calculated with B3LYP is relatively smaller, while the emission wavelength calculated with M06-2X is in good agreement with the experimental value. As we

Table 1
Excited energy of the S1 state and the T1 state for the 2CzPN molecule calculated with the TD-DFT method at various functional levels. The energy gap between the S1 and T1 states, the oscillator strength of the S1 state and the emission wavelengths are also presented.

2CzPN	B3LYP	CAM-B3LYP	PBE0	M06-2X	WB97X-D
ΔE_{ST}(eV)	0.01	0.92	0.14	0.86	0.39
f	0.0001	0.0001	0.0001	0.0047	0.0057
λ_{em}(nm)	672	423	615	446	409

mentioned above, M06-2X may give better description of the geometry of the 2CzPN molecule than other functionals. Further, we deduce that the 'hybrid' method with the geometry optimized with M06-2X and the energy calculated with B3LYP may give good description of electronic structure of the system. With this 'hybrid' method, the S-T energy gap calculated is 0.139 eV, which is more reasonable for a TADF emitter. The rationality of the 'hybrid' method can also be confirmed by the 4CzIPN molecule and the 4CzPN molecule studied as follows.

3.2. Systematic study on the electroluminescent mechanism of the 4CzIPN molecule

The photophysical property of molecules is basically determined by their geometric structures and the structures of the energy states. For the 4CzIPN molecule, the geometry of the S1 and T1 states optimized with B3LYP change significantly compared with the S0 state. For both the S1 and T1 states, the dihedral angles (**da1**, **da2** and **da3**) are close to 90°, while the three angles for the S0 state are about 60° (see Table S2). The large difference between the S0 and S1 states may result in weak overlap between two states, and consequently one can't observe strong fluorescence from the molecule. The geometries for the three states optimized with M06-2X do not have significant differences. The difference of dihedral angles between S1 (T1) and S0 is no more than 5°. The geometries of 4CzIPN at S0, S1 and T1 states optimized with B3LYP are quite different with those optimized with M06-2X (see Fig. S4 and Fig. S5). The four dihedral angles (**da1**, **da2**, **da3** and **da4**) in three states (S0, S1, T1) optimized with B3LYP is larger than that optimized with M06-2X (see Fig. 1(b) and Table S2). Especially for the S1 and T1 states obtained with B3LYP, the surfaces of the carbazolyls and the dicyanobenzene are almost perpendicular. However, for the S1 and T1 states optimized with M06-2X, the dihedral angles between the surfaces of the carbazolyls and the dicyanobenzene are more or less than 50°. From the top view of the S1 state optimized with B3LYP and M06-2X, we can see that the relative positions of the carbazolyls and the dicyanobenzene are totally different. In the latter, the carbazolyls at the up and the down positions are parallel with each other ('P' form), while they adapt the 'X' form in the former situation (Fig. 2 (a) and (b)). Besides, we can also note that the dihedral angles of 94-1-72-73 and 93-3-53-52 are quite small for the B3LYP result (almost plane), while they become larger for the geometry optimized with M06-2X. The similar situation can also be seen for the 2CzPN molecule (see Table S1) and the 4CzPN molecule (see Table S3).

Theoretical calculation finds that the carbazolyls are very flexible and easy to rotate around the C–N bonds. Thus, it is interesting to investigate the energy surface variation when the dihedral angle **da4** is changed. It is obvious that the dihedral angle **da4** is much more flexible than the other three dihedral angles due to the steric hindrance of the carbazolyls. The energy surface of the molecule with different dihedral angles of **da4** is studied and the results are shown in Fig. 2(c) and (d). The potential energy curve is scanned at the M06-2X level, and the energy potential curve of the S1 state is also obtained by the vertical excitation calculation (Fig. 2(c) and (d)). It is clear that the energy is the lowest when the dihedral angle is 60.59° for the S0 state, where the two carbazolyls at the up and down positions are parallel with each other ('P' configuration, see Fig. 2(f) and (g)). There is also another local minimum for the S0 state when the dihedral angle is 115.59° with the two carbazolyls at the up and down positions in the form of 'X' (see Fig. 2(j) and (k)). From the potential energy surface of the S0 state, one can see that the energy barrier for the molecule to change from 'P' to 'X' configuration is only 54 meV. With the help of thermal fluctuation, the molecule may change from the 'P' to the 'X' configuration. One

can also note that energy barrier for the 'X' configuration to go to the 'P' configuration is even small, with only 23 meV. That is to say, the 'X' configuration can easily change to the 'P' configuration at the room temperature. A similar picture can be seen in the potential energy curve of the S1 state. The barrier for the S1 state from the 'P' configuration to the 'X' configuration is 116 meV, while the reverse barrier is about 32 meV. From Fig. 2(d), one can see that the lowest point is located at the 55.59° for the S1 state, which is slightly smaller than the angle in the S0 state. Both of them are consistent with the optimized results (57.77° for the S1 state and 60.59° for the S0 state). Fig. 2 (e) presents the oscillator strength excited from the S0 state to the S1 state of the 4CzIPN molecule at different dihedral angles of **da4**. It is indicated that the oscillator strength is relatively smaller than the popular fluorescent materials (usually larger than 1.0), and the smallest oscillator strength is found at the most stable point. Consequently, weak fluorescent strength is predicted for the 4CzIPN molecule.

The same as the 2CzPN molecule, there are significant differences between the geometry optimized with B3LYP and M06-2X for the 4CzIPN molecule. The simulation of the absorption spectra and emission spectra may provide a useful way to check the suitability of the functional for the system. The first absorption peak for the 4CzIPN molecule calculated with B3LYP is 500 nm, which is about 50 nm larger than the experimental result (see Table 2). It is 370 nm calculated with M06-2X, which is much smaller than the experimental value. It is noticeable that the Stoke shift between the emission and absorption spectra is 52 nm calculated with M06-2X, which agrees with the experimental result quite well. However, the Stoke shift calculated with B3LYP is as large as 225 nm, which has large discrepancy with the experimental result. It is understandable, since the geometry of the S1 changes a lot compared with the S0 state obtained with B3LYP. While the difference between the S1 and S0 states obtained with M06-2X is much smaller. From the absorption spectra and emission spectra, we conclude that the M06-2X functional can well describe the geometry of this kind of systems and B3LYP can give relatively better energy prediction, which is in consistent with the result of the 2CzPN molecule. Consequently, a 'hybrid' method is adopted. In Fig. 3, the absorption spectra and the emission spectra as well as the oscillator strength calculated with the 'hybrid' method are illustrated (one can also see Table 2). The first absorption position is located at the 474 nm, which is quite close to the experimental value (450 nm). The peak value of the emission spectra is 569 nm, and it also agrees with the experimental result (507 nm) quite well. It further confirms the suitability of the 'hybrid' method, and we will use this method in all the following calculations.

The S-T energy gap is one important factor that determines whether the RISC can be realized. In our calculation, the S-T energy gap for the 4CzIPN molecule is 43.3 meV (see Table 3), which is in good agreement with the experimental result. The reorganization energy is 188.0 meV and the spin orbit coupling is 0.49 cm^{-1}. Obviously, the spin orbit coupling is still small as other organic molecules reported before [13]. However, the small S-T energy gap can make the RISC realized easily. According to the Marcus rate equation, we can obtain the RISC rate (8.99×10^6 s^{-1}). The ISC rate is 4.85×10^7 s^{-1}, a little larger than the RISC rate. As the S-T energy gap and the spin-orbit coupling are two important parameters to determine the RISC rate, the relationship between them and the (R)ISC rate is investigated. It can be seen that the ISC rate first increases, then decreases with the broadening of the S-T energy gap, while the RISC rate becomes to zero fast with the S-T energy gap increasing (see Fig. 4(a)). This is due to different active energies produced for the two processes. From Fig. 4(b), we will see that the relationship between the (R)ISC rate and the spin-orbit coupling presents in the form of a parabolic curve. With the enhancement of
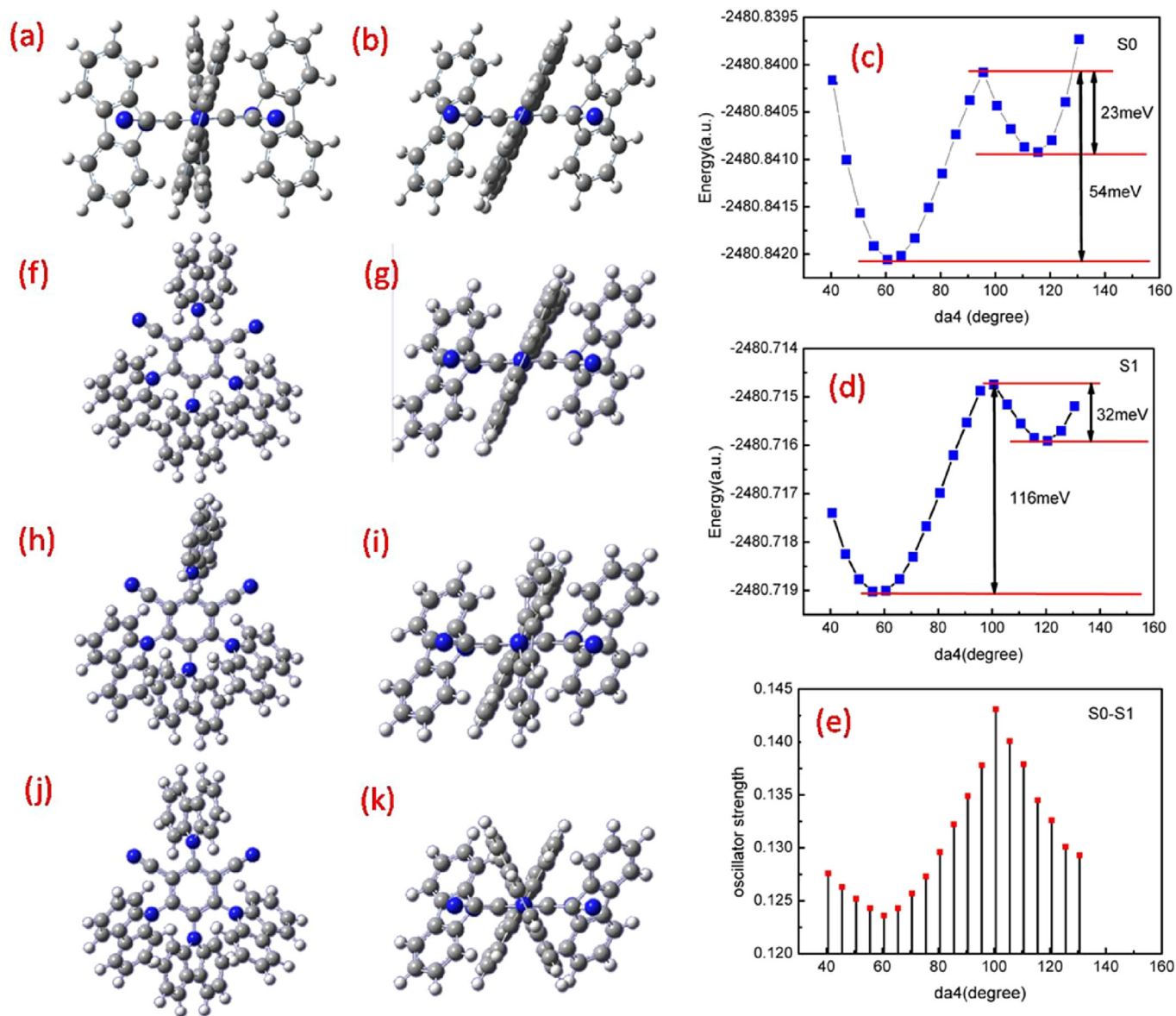
Fig. 2. (a) and (b) top view of the S1 state of the 4CzIPN molecule optimized with B3LYP and M06-2X respectively; (c) and (d) are potential energy curves of the S0 state and the S1 state of the 4CzIPN molecule with the dihedral angle **da4** changing from 40.59° to 140.59°; (e) Oscillator strength for the 4CzIPN molecule excited from the S0 state to the S1 state when the dihedral angle **da4** of the S0 state changes. (f) and (g) are the side view and the top view of the 4CzIPN molecule with **da4** as 60.59°; (h) and (i) are the side view and the top view of the 4CzIPN molecule with **da4** as 95.59°; (j) and (k) are the side view and the top view of the 4CzIPN molecule with **da4** as 115.59°.

Table 2
Absorption and emission wavelengths for the 4CzIPN and 4CzPN molecule. The experimental value and the values calculated with B3LYP, M06-2X and the 'hybrid' method are also shown. (unit: nm).

	4CzIPN		4CzPN	
	λ_{ab}	λ_{em}	λ_{ab}	λ_{em}
Experimental value	450	507	—	530
B3LYP	500	725	505	793
M062X	370	422	363	449
'Hybrid' method	474	569	479	651

the spin-orbit coupling, both transition rates increase fast.

Besides the (R)ISC rate, the radiation rate of S1 state is also calculated, which is in the same order with the ISC rate. The non-radiation rate of the T1 state and the phosphorescence rate are 0.375 s^{-1} and 0.309 s^{-1}, and both of them are very small. One should note that the non-radiation rate of the S1 state is 2.33×10^5 s^{-1}, which is only one order of magnitude smaller than the radiation rate. This is due to the flexibility of the molecule, which can induce significant vibration relaxation of the molecule. Thus, it is quite delicate for the molecule design to obtain a TADF emitter. From the rate calculation, we can deduce that the RISC process will proceed successfully. To confirm the conclusion, the rate equation is used to study the evolution process. In the equation, the initial occupation density of the S1, T1 and S0 states are assumed as 0.25, 0.75 and 0.0, and the triplet-triplet annihilation is not in consideration here. The evolutionary process of the three states is shown in Fig. 4(c). It is indicated that all the states tend to dynamic equilibrium after 3μs. Specifically, the occupation density in the S1 states decreases rapidly at first, then it becomes slowly to zero. The occupation density in T1 states increases first, then decreases to
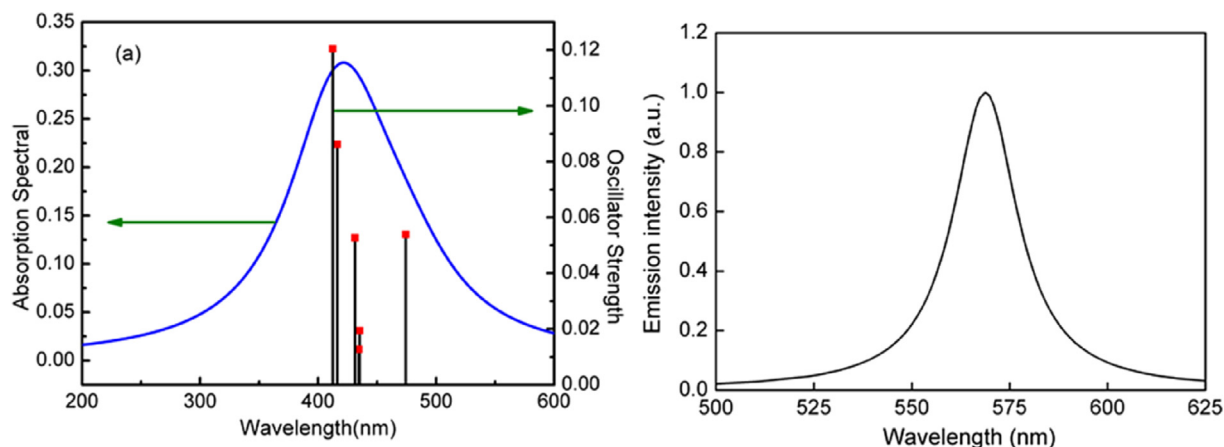
Fig. 3. (a) and (b) Absorption spectra and emission spectra for the 4CzIPN molecule calculated with the 'hybrid' method. The oscillator strength has also been presented.

Table 3
Energy gap between the S1 and T1 states for the 4CzIPN molecule and the 4CzPN molecule. The reorganization energy and spin orbit coupling between the S1 and T1 states are also shown. In addition, the oscillator strengths for the S1 state of two molecules are listed as well. The radiation rate of the S1 state, the intersystem crossing rate and the reverse intersystem crossing rate are presented.

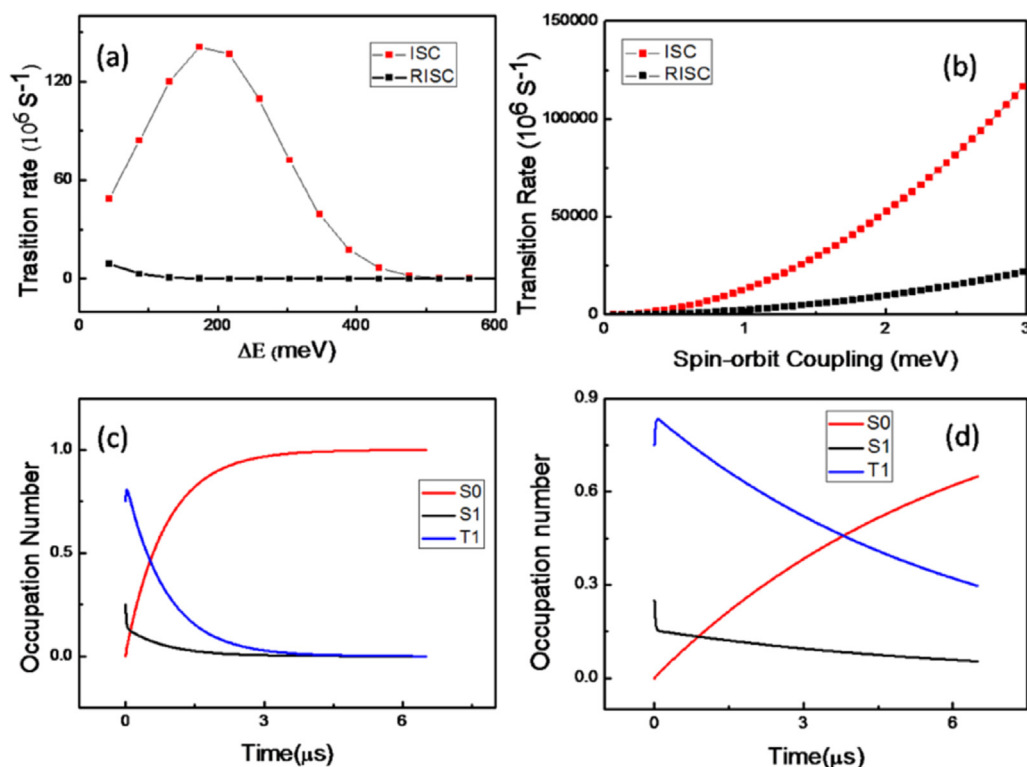| System	ΔE_{ST}(meV)	λ(meV)	V_{SO} (cm^{-1})	f	k_{S1-S0} (s^{-1})	k_{S1-T1}^{ISC} (s^{-1})	k_{T1-S1}^{RISC} (s^{-1})
4CzIPN	43.0	188.0	0.49	0.054	8.12×10^6	4.85×10^7	9.00×10^6
4CzPN	39.0	220.5	0.801	0.019	2.98×10^6	8.24×10^7	1.81×10^7

Fig. 4. (a) Relationship of the (R)ISC rate for the 4CzIPN molecule with the S-T energy gap; (b) Relationship of the (R)ISC rate for the 4CzIPN molecule with the spin-orbit coupling; (c) Evolution process of the S1, T1 and S0 states for the 4CzIPN molecule with initial occupation number 0.25, 0.75 and 0.0 respectively; (d) Evolution process of the S1, T1 and S0 states for the 4CzIPN molecule when the radiation rate of the S1 state is assumed as 8.1×10^5 s^{-1}.

zero too. However, the density in S0 state increases all the way and becomes to one at last. That is to say, all excitons in the S1 state will decay to the S0 state although some singlet excitons decay to the triplet excitons first. Due to the phosphorescence rate and the non-radiation rate of the T1 state are quite small, the triplet excitons can successfully up-convert to singlet excitons by the RISC process

before they decay to the S0 state. This confirms that the up-conversion of the T1 state to the S1 state can be realized for the 4CzIPN molecule. This is due to the good balance of the dynamics of all the processes involved in the three states. If the radiation rate of the S1 state is one order smaller than the calculated value, we can see that the three states can't be in equilibrium in the limited time (see Fig. 4(d)). This is because that the S1 state is not fast enough to decay to the ground state in time and most of them convert to the T1 state. It is indicated that large radiation rate of S1 is a necessary condition for the realization of delayed fluorescence, while it is quite a challenge for the D-A type based molecules. The 4CzIPN molecule can effectively satisfy this condition and we will analysis its character of excited states in the following section.

The electron and hole distribution of the S1 state for the 4CzIPN molecule is shown in Fig. 5(a). It is indicated that electrons mainly located at the central dicyanobenzene (A) group, while holes are distributed at the four carbazolyls (D) group. It means electrons transfer from the D groups to the central A groups when the molecule is excited to the S1 state. This can also be confirmed by analyzing the natural transition orbitals (NTO) of S1 (shown in Fig. 5(c)) which shows significant CT characteristics. In addition, it is also illustrated that there is some overlap between two transition orbitals in the central area. As shown in Fig. 5(b), the diagram of the overlap of electrons-hole indicates that overlap area is mainly located at the benzene ring. That is to say, the S1 has some contribution from the localized excitation (LE). As we know, overlap

between two transition orbitals is one necessary condition for the fluorescent emission, and the separation of two transition orbitals can induce small S-T energy gap. The combined characteristic of the S1 state for the 4CzIPN molecule makes it satisfy the requirement that the S-T energy gap is small and the radiation rate is large enough. From Table 2, we can see that the radiation rate of the S1 state for the 4CzIPN molecule is 8.12×10^6 s^{-1}, which is smaller than normal organic fluorescent molecules. This is a common shortcoming of this kind of TADF emitters. Nevertheless, some attempts to enhance the fluorescent intensity of the TADF emitters have been performed [3c], and we are also working on this direction now.

3.3. Isomer effect

The 4CzPN molecule, which is the isomer of the 4CzIPN molecule, is also studied with both B3LYP and M06-2X as well as the 'hybrid' method. The geometries of the 4CzPN molecule optimized with B3LYP and M06-2X are shown in the Fig. S6 and S7 respectively. The geometry obtained with B3LYP still assumes the symmetric structure, which is consistent with the results above. One can refer to Table S3 to see the detail structure information. For comparison, we list some important parameters calculated with the 'hybrid' method that can influence the delayed fluorescence (see Table 3). It is indicated that the S-T energy gap for the 4CzPN molecule is only 39 meV, a little smaller than that of 4CzIPN
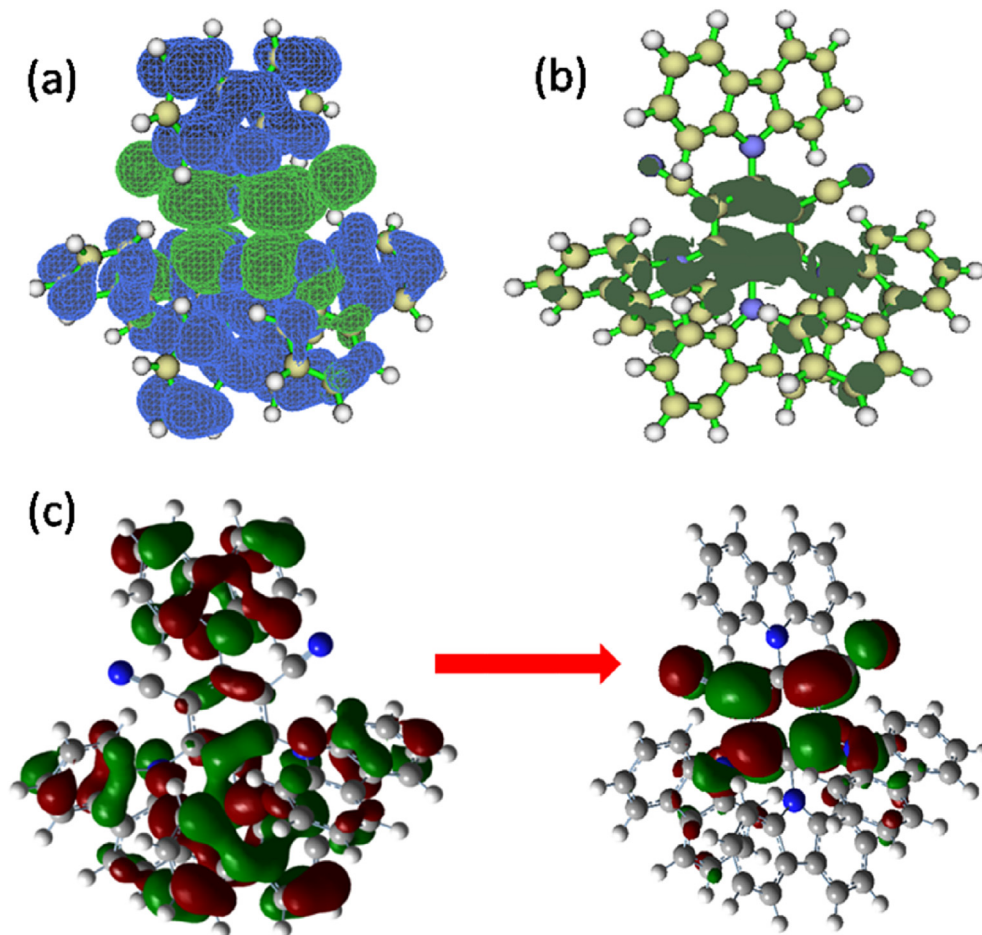

Fig. 5. (a) Electron-hole distribution of the S1 state for the 4CzIPN molecule, and the blue color and green color represent holes and electrons respectively; (b) Overlap of electron-hole for the S1 state of the 4CzIPN molecule; (c) Natural transition orbitals of the S1 state for the 4CzIPN molecule. (For interpretation of the references to colour in this figure legend, the reader is referred to the web version of this article.)

molecule. In addition, the SOC of the 4CzPN molecule is about two times of that of 4CzIPN, thus a faster ISC rate for the 4CzPN molecule is expected. The calculated value is 8.24×10^7 s^{-1}, about two times of the ISC rate for the 4CzIPN molecule. The similar relationship is also found for the RISC rate. The RISC rate for the 4CzIPN molecule is only about one half of the rate for the 4CzPN molecule. However, the emission rate of the S1 state for the 4CzPN molecule is 2.98×10^6 s^{-1}, which is about 3 times smaller than that of the 4CzIPN molecule. That may be the reason why the internal quantum efficiency of the 4CzPN molecule is a little smaller than that of the 4CzIPN molecule. In comparison with the 4CzIPN molecule, the only difference is that the positions of the carbazolyl groups and the cyano groups on the benzene rings. In the 4CzIPN molecule, the cyano groups are at the adjacent position in the benzene ring. They are separated by the carbazolyl group. The different arrangement of donor and acceptors will induce different charge transfer properties in the excited states, thus different oscillator strength and S-T energy gap. Based on the results of these two molecules, we can find that the separate arrangement of donors and acceptors will result in a wide S-T energy gap but large oscillator strength. In addition, the emission wavelength of the 4CzPN molecule is about 651 nm (experimental value: 525 nm), which shows red shift than the emission spectra of the 4CzIPN molecule (see Table 2). It further indicates that changing of the relative positions of the D and A groups will also influence its emission color.

4. Conclusions

In summary, TD-DFT method is used to study the geometric and electronic property of excited states for three D-A type molecules. Five kinds of functionals are tested on the 2CzPN molecule, and a 'hybrid' method with geometry optimized using M06-2X and energy calculated with B3LYP is proposed. With this 'hybrid' method, systematic investigation on the 4CzIPN molecule is performed and double-well potential energy surfaces are found for both the S0 and S1 states. Due to the energy barrier is quite shallow, both stable configurations can convert to each other easily even at room temperature. The absorption spectra and the emission spectra of the 4CzIPN molecule agree with the experimental results quite well, which further confirms the rationality of the 'hybrid' method. Based on the energy state structure of the 4CzIPN molecule, three states including the S0, S1 and T1 states are used to study the up-conversion mechanism. The dynamic of the excited states shows that the RISC rate is large enough to make the T1→S1 up-conversion realized. By using the phenomenological rate equation, one can get a better understanding of the evolution process of the excitons. Further analysis of the transition orbitals of the excited states indicates that the S1 states of the TADF emitters possess both CT and LE component, and rational proportion of LE and CT components are important for the design of a high efficient TADF emitter. Comparing the properties of two isomers (4CzPN and 4CzIPN), we find that separate arrangement of donors and acceptors will result in a wide S-T energy gap but large oscillator strength, and also the blue shift of the emission spectra.

Acknowledgment

Appendix A. Supplementary data

Supplementary data related to this article can be found at http://dx.doi.org/10.1016/j.orgel.2016.11.035.

References

[1] L.J. Rothberg, A.J. Lovinger, Status of and prospects for organic electroluminescence, J. Mater. Res. 11 (1996) 3174—3187.
[2] H. Uoyama, K. Goushi, K. Shizu, H. Nomura, C. Adachi, Highly efficient organic light-emitting diodes from delayed fluorescence, Nature 492 (2012) 234—238.
[3] (a) I.S. Park, M. Numata, C. Adachi, T. Yasuda, A phenazaborin-based high-efficiency blue delayed fluorescence material, B. Chem. Soc. Jap. 89 (2016) 375—377;
(b) K. Shizu, H. Kaji, Organic electroluminescent materials realizing efficient conversion from electricity to light, J. Photopolym. Sci. Tec. 29 (2016) 305—310;
(c) D.R. Lee, B.S. Kim, C.W. Lee, Y. Im, K.S. Yook, S.H. Hwang, J.Y. Lee, Above 30% external quantum efficiency in green delayed fluorescent organic light-emitting diodes, Acs. Appl. Mater. Inter. 7 (2015) 9625—9629;
(d) Q.S. Zhang, B. Li, S.P. Huang, H. Nomura, H. Tanaka, C. Adachi, Efficient blue organic light-emitting diodes employing thermally activated delayed fluorescence, Nat. Photonics. 8 (2014) 326—332;
(e) Q. Zhang, H. Kuwabara, W.J. Potscavage Jr., S. Huang, Y. Hatae, T. Shibata, C. Adachi, Anthraquinone-based intramolecular charge-transfer compounds: computational molecular design, thermally activated delayed fluorescence, and highly efficient red electroluminescence, J. Am. Chem. Soc. 136 (2014) 18070—18081;
(f) L. Yao, S. Zhang, R. Wang, W. Li, F. Shen, B. Yang, Y. Ma, Highly efficient near-infrared organic light-emitting diode based on a butterfly-shaped donor—acceptor chromophore with strong solid-state fluorescence and a large proportion of radiative excitons, Angew. Chem. 126 (2014) 2151—2155;
(g) H. Wang, L. Xie, Q. Peng, L. Meng, Y. Wang, Y. Yi, P. Wang, Novel thermally activated delayed fluorescence materials—thioxanthone derivatives and their applications for highly efficient OLEDs, Adv. Mater 26 (2014) 5198—5204;
(h) H. Nakanotani, T. Higuchi, T. Furukawa, K. Masui, K. Morimoto, M. Numata, H. Tanaka, Y. Sagara, T. Yasuda, C. Adachi, High-efficiency organic light-emitting diodes with fluorescent emitters, Nat. Commun. (2014) 5;
(i) S. Zhang, W. Li, L. Yao, Y. Pan, F. Shen, R. Xiao, B. Yang, Y. Ma, Enhanced proportion of radiative excitons in non-doped electro-fluorescence generated from an imidazole derivative with an orthogonal donor—acceptor structure, Chem. Commun. 49 (2013) 11302—11304;
(j) S. Wu, M. Aonuma, Q. Zhang, S. Huang, T. Nakagawa, K. Kuwabara, C. Adachi, High-efficiency deep-blue organic light-emitting diodes based on a thermally activated delayed fluorescence emitter, J. Mater. Chem. C 2 (2013) 421—424;
(k) K. Sato, K. Shizu, K. Yoshimura, A. Kawada, H. Miyazaki, C. Adachi, Organic luminescent molecule with energetically equivalent singlet and triplet excited states for organic light-emitting diodes, Phys. Rev. Lett. 110 (2013) 247401;
(l) H. Nakanotani, K. Masui, J. Nishide, T. Shibata, C. Adachi, Promising operational stability of high-efficiency organic light-emitting diodes based on thermally activated delayed fluorescence, Sci. Rep. 3 (2013) 2127;
(m) W. Li, Y. Pan, R. Xiao, Q. Peng, S. Zhang, D. Ma, F. Li, F. Shen, Y. Wang, B. Yang, Employing~ 100% excitons in OLEDs by utilizing a fluorescent molecule with hybridized local and charge-transfer excited state, Adv. Funct. Mater. 24 (2014) 1609—1614;
(n) J. Li, T. Nakagawa, J. MacDonald, Q.S. Zhang, H. Nomura, H. Miyazaki, C. Adachi, Highly efficient organic light-emitting diode based on a hidden thermally activated delayed fluorescence channel in a heptazine derivative, Adv. Mater. 25 (2013) 3319—3323;
(o) F.B. Dias, K.N. Bourdakos, V. Jankus, K.C. Moss, K.T. Kamtekar, V. Bhalla, J. Santos, M.R. Bryce, A.P. Monkman, Triplet harvesting with 100% efficiency by way of thermally activated delayed fluorescence in charge transfer OLED emitters, Adv. Mater. 25 (2013) 3707—3714;
(p) X.-L. Chen, R. Yu, Q.-K. Zhang, L.-J. Zhou, X.-Y. Wu, Q. Zhang, C.-Z. Lu, Rational design of strongly blue-emitting cuprous complexes with thermally activated delayed fluorescence and application in solution-processed OLEDs, Chem. Mater. 25 (2013) 3910—3920;
(q) K. Goushi, K. Yoshida, K. Sato, C. Adachi, Organic light-emitting diodes employing efficient reverse intersystem crossing for triplet-to-singlet state conversion, Nat. Photonics. 6 (2012) 253—258, 1;
(r) P. Chen, L.P. Wang, W.Y. Tan, Q.M. Peng, S.T. Zhang, X.H. Zhu, F. Li, Delayed fluorescence in a solution-processable pure red molecular organic emitter based on dithienylbenzothiadiazole: a joint optical, electroluminescence, and magnetoelectroluminescence study, Acs Appl. Mater Inter 7 (4) (2015) 2972—2978.

[4] Q. Peng, W. Li, S. Zhang, P. Chen, F. Li, Y. Ma, Evidence of the reverse inter-system crossing in intra-molecular charge-transfer fluorescence-based organic light-emitting devices through magneto-electroluminescence measurements, Adv. Opt. Mater. 1 (2013) 362–366.

[5] (a) X. Cai, X. Li, G. Xie, Z. He, K. Gao, K. Liu, D. Chen, Y. Cao, S.-J. Su, "Rate-Limited effect" of reverse intersystem crossing process: the key for tuning thermally activated delayed fluorescence lifetime and efficiency roll-off of organic light emitting diodes, Chem. Sci. 7 (2016) 4264–4275;
(b) K. Shizu, H. Tanaka, M. Uejima, T. Sato, K. Tanaka, H. Kaji, C. Adachi, Strategy for designing electron donors for thermally activated delayed fluorescence emitters, J. Phys. Chem. C 119 (2015) 1291–1297.

[6] M. Frisch, G. Trucks, H. Schlegel, G. Scuseria, M. Robb, J. Cheeseman, G. Scalmani, V. Barone, B. Mennucci, G. Petersson, et al., Gaussian 09, Revision a. 02, Gaussian Inc., Wallingford, CT, 2009.

[7] T. Lu, F.W. Chen, Multiwfn: a multifunctional wavefunction analyzer, J. Comput. Chem. 33 (2012) 580–592.

[8] A. Einstein, Zur quantentheorie der strahlung, Phys. Z. 18 (1917) 121–128.

[9] Shuai, Z. G.; Peng, Q.; Niu, Y. L.; Geng, H. MOMAP, a Free Andopen-source Molecular Materials Property Prediction Package; Revision 0.2.004; available online: http://www.shuaigroup.net/, Beijing, China, 2014.

[10] (a) Y. Niu, Q. Peng, Z. Shuai, Promoting-mode free formalism for excited state radiationless decay process with duschinsky rotation effect, Sci. China, Ser. B Chem. 51 (2008) 1153–1158;
(b) Q. Peng, Y. Yi, Z. Shuai, J. Shao, Toward quantitative prediction of molecular fluorescence quantum Efficiency: role of duschinsky rotation, J. Am. Chem. Soc. 129 (2007) 9333–9339;
(c) Q. Peng, Y. Yi, Z. Shuai, J. Shao, Excited state radiationless decay process with duschinsky rotation effect: formalism and implementation, J. Chem. Phys. 126 (2007) 114302.

[11] O. Vahtras, H. Ågren, P. Jo/rgensen, H.J.R.A. Jensen, T. Helgaker, J. Olsen, Multiconfigurational quadratic response functions for singlet and triplet perturbations: the phosphorescence lifetime of formaldehyde, J. Chem. Phys. 97 (1992) 9178–9187.

[12] Dalton2011, a Molecular Electronic Structure Program, 2011 see, http://www.daltonprogram.org.

[13] D. Beljonne, Z. Shuai, G. Pourtois, J.L. Bredas, Spin–orbit coupling and inter-system crossing in conjugated Polymers: a configuration interaction description, J. Phys. Chem. A 105 (2001) 3899–3907.